ce/papers Proceedings in civil engineering

Ernst & Sohn A Wiley Brand

ORIGINAL ARTICLE

EUROSTRUCT

STRUCTURAL HEALTH MONITORING OF CURVED ROADWAY BRIDGES THROUGH SATELLITE RADAR INTERFEROMETRY AND COLLAPSE SIMULATION

Elisabetta Farneti[1] | Andrea Meoni[1] | Agnese Natali[2] | Simone Celati[2] | Carmine Frascella[3] | Maria Cristina Lupi[3] | Nicola Cavalagli[1] | Ilaria Venanzi[1] | Walter Salvatore[2] | Filippo Ubertini[1]

Correspondence

Ms. Elisabetta Farneti
Department of Civil and Environmental Engineering
University of Perugia
Via G. Duranti 93
06125 Perugia, Italy
Email: elisabetta.farneti@studenti.unipg.it

[1] University of Perugia, Perugia, Italy
[2] University of Pisa, Pisa, Italy
[3] e-GEOS SpA, Roma, Italy

Abstract

This paper presents the application of a Structural Health Monitoring (SHM) strategy for bridges affected by slow deformation phenomena to a curved roadway bridge undergoing slow landslide-induced movements. The chosen multidisciplinary approach is based on the combination of remote sensing data through satellite Synthetic Aperture Radar Interferometry (InSAR) and structural analysis up to collapse investigated through the Applied Element Method (AEM). The results of the application to the considered case study demonstrate that the integration of the displacement information obtained through InSAR technique with the numerical analysis allows for improving the comprehension of the health state of the bridge undergoing slow movements and identifying potentially critical conditions for the structure.

Keywords

Structural Health monitoring, bridges, remote sensing, SAR interferometry, numerical analysis, applied element method

1 Introduction

Since bridges constitute an irreplaceable portion of the infrastructural transport network, their preservation is fundamental from an economic, social and often historical point of view. A large number of European bridges has been in service for more than half a century and, during their lifetime, they have undergone significant increases of the traffic loads, as well as material degradation and damage due to extreme events or slow deformation phenomena. The assessment of the health state of bridges is therefore imperative to preserve their functionalities and optimize maintenance activities.

In this framework, Structural Health Monitoring (SHM) strategies [1-5], based on the analysis of data collected by contact or contactless sensors, play a key role in the early detection of damage and evaluation of the current condition of the structures, and a multidisciplinary approach is fundamental to obtain heterogeneous and complementary information. Recently, among the various technologies used for SHM purposes, Synthetic Aperture Radar Interferometry (InSAR) has emerged as a powerful tool for following the evolution of the movements of buildings and infrastructures [6-11]. InSAR techniques exploit data acquired by satellites orbiting at a distance from the Earth's surface of more than 500 km and are especially suitable for monitoring slow deformations, due to the dependence of the measurements on the revisit time of the satellite over the area of interest. Through InSAR it is possible to monitor a large number of infrastructures at relatively low costs thanks to the coverage of wide regions without the need to install instrumentation on site or even access the study site. Starting from SAR observations acquired from two different viewing geometries of the satellite radar antenna, it is possible to derive a two-dimensional projection of the movement of a bridge over time and quantify the uncertainties on the estimated displacements [12].

When aiming at performing a structural prognosis based on monitoring data, it is mandatory to integrate such data with advanced numerical analyses that allow building a digital twin of the structure able to replicate the non-linear behaviour of its physical counterpart and the propagation

https://doi.org/10.1002/cepa.2201

of damage, in order to predict the conditions under which the collapse of the bridge may occur. This knowledge, in support of the information provided by monitoring systems, is essential for interpreting the current state of the structure and for deciding whether it is necessary to implement interventions aimed at avoiding major accidents. Among the different computational strategies, the recently proposed Applied Element Method (AEM) [13-15] satisfies the need to simulate both continuum and discrete stages of a structure that progressively reaches collapse, tracking the behaviour from the elastic stage to cracking, crushing, yielding of reinforcements, element separation and collision [16-19].

This work presents a combined use of InSAR-based monitoring and AEM numerical analysis for the structural assessment of a curved roadway bridge, undergoing a slow deformation phenomenon consisting of movements induced by a slowly evolving landslide.

2 Case study

The bridge chosen as case study is a pre-stressed concrete bridge with post-tensioned cables, located in Italy and built over a river in the late 1970s (Figure 1).

It has a curvilinear planimetric trend and the axis of the deck can be identified by an arc of a circle having a radius of about 36.25 m (see the plan views in Figure 2 and Figure 3). The bridge has an overall length of 66 m and consists of three spans, of which the central one is 36 m long while the two lateral ones develop over a length of 15 m each. The static scheme which characterizes the structure is the continuous beam on four supports. The two piers constituting the intermediate supports consist of two reinforced concrete elements one over the other: the lower one is the foundation of the pier, while the upper one is connected to the bridge deck and foundation through cylindrical hinge constraints, therefore having a pendulum behaviour. Mobile bearing supports are present between the deck and the left side abutment in Figure 1, while the other abutment is seat of a fix constraint with the deck.

As previously mentioned, the bridge is subjected to slow movements caused by a landslide affecting the slope on which an abutment and a pier are founded called from now on abutment 1 and pier 1 (left side in Figure 1). The deformations, already highlighted during the construction phase of the bridge, continued up to date, causing a progressive movement towards the valley of abutment 1 and pier 1. The evolution of these deformations over time caused the closure of the joint between the deck and the ballast wall of abutment 1, facilitated by the presence of the mobile bearing supports and resulting in a thrust of abutment 1 on the deck. Both pier 1 and pier 2 underwent longitudinal and transverse rotations, even if less significant for pier 2. The rotation around the longitudinal axis of the deck brought to the elevation of the downstream corner of the piers previously leaned on the foundation base. The induced translation of the deck also resulted in the crisis of the ballast wall of abutment 2 (right side in Figure 1).

Over the years, measures were implemented to mitigate the deformation phenomenon in progress. In 2019, an important intervention allowed to temporarily eliminate the thrust of abutment 1 on the deck, by reopening the joint through the creation of a gap of 30 cm between the slab and the ballast wall. In this way no further pressure is immediately exerted on the deck due to the movements of the slope. Other countermeasures against the effects of the advancement of the landslide and to improve the stability of the slope have been designed. In addition, a static monitoring system has been installed on the bridge and the slope affected by the landslide, in order to follow the evolution of the deformations.

Figure 1 Case study: curved roadway bridge in Italy.

3 InSAR analysis

The Italian satellite constellation COSMO-SkyMed acquired over the area of interest two stacks of SAR images in double geometry (ascending, when the satellite travels approximately from South to North poles, and descending, when it navigates from North to South poles) with a spatial resolution of 3×3m. The first dataset consists of 51 images acquired in ascending viewing geometry in the period January 2018-December 2021, while the second one is composed by 78 images recorded in the time span between January 2018 and January 2022 in descending pass.

The two datasets have been processed through Persistent Scatterer Pair (PSP) technique [20], obtaining the displacement information for a set of sparse points on the bridge deck and on the neighbouring ground, called Persistent Scatterers (PSs), and corresponding to radiometrically stable targets over the monitoring period. The displacement measurements thus derived have a millimetre-scale precision, while the PSs are localized in the three-dimensional space with metric precision.

The provided measurements are actually the projections of the real displacement vectors along the so-called Line-Of-Sight (LOS), which connects the satellite radar antenna with the target on the ground in the considered viewing geometry. Figure 2 shows the ascending and descending velocity maps of the PSs detected on the deck of the bridge. In both geometries, for the PSs identified on the portion of the deck on the side of abutment 1 and pier 1, the temporal evolution of the displacements in the monitoring time window highlights a trend with a clear accumulation of irreversible deformations.

Even though the displacement measurements along the LOS themselves provide information helping to recognize a potentially critical condition for the bridge, it is convenient to convert them into displacement components along

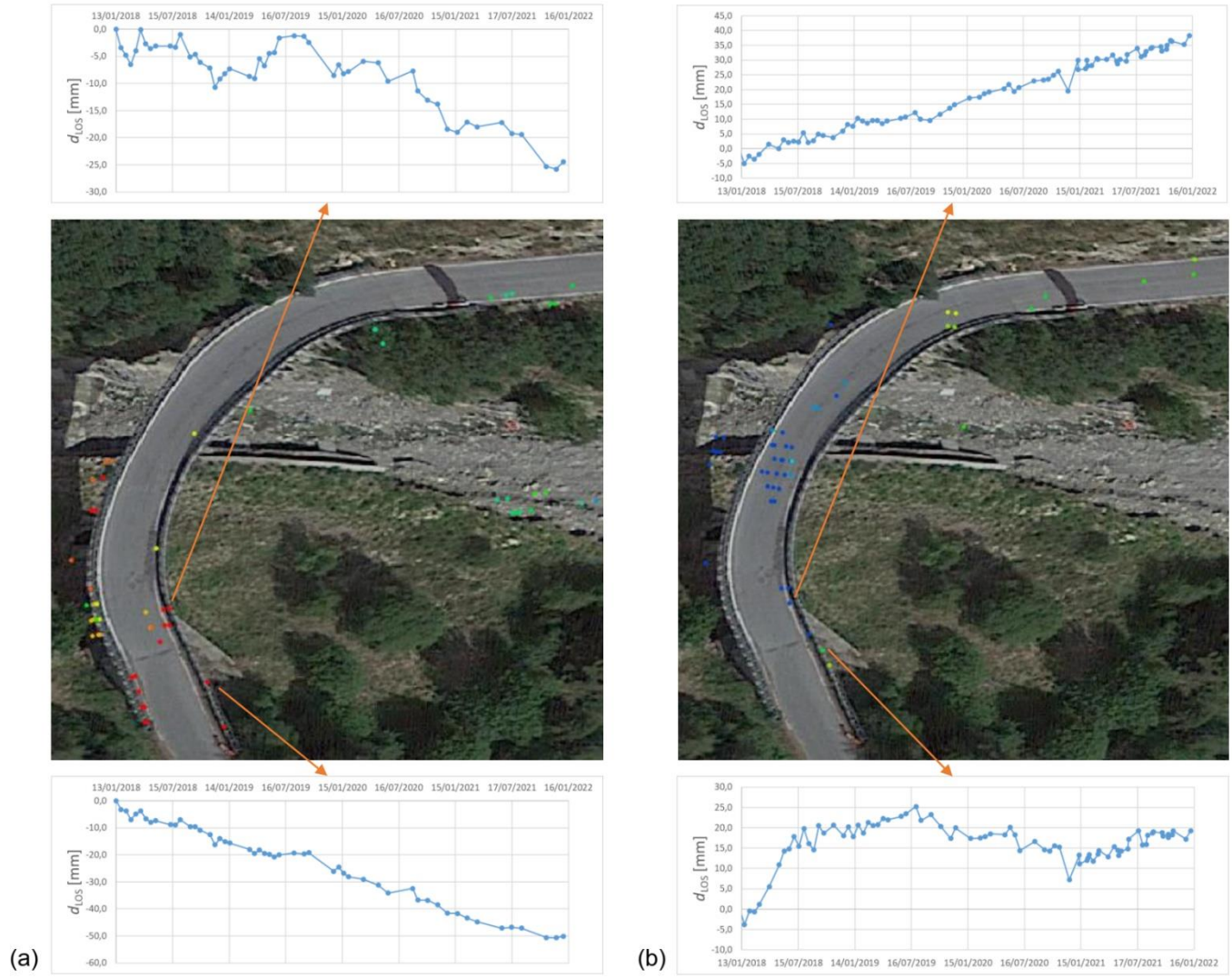

Figure 2 PSs detected in (a) ascending and (b) descending geometry on the bridge deck, color-coded based on their mean velocity in the monitored period (positive values indicate movements towards the sensor); in both geometries the time series of two PSs are shown, identified on portions of the deck above abutment 1 and pier 1, respectively.

more significant directions for the bridge, in order to better understand and interpret the nature of the movements involved. Having available measurements along two different LOS, which constitute a two degree-of-freedom information, it is not possible to carry out a complete reconstruction of the three dimensional displacement field, but only to estimate two components of the real displacement vector, which is equivalent to hypothesizing the plane on which the deformation occurs. In order to obtain this result, a post-processing procedure developed by Farneti et al. [12] is used in this work, which allows to estimate 2D displacements of a bridge on a chosen deformation plane starting from ascending and descending acquisitions with proper defined error bounds. The application to the case under examination is described below, while the interested reader can find more details of the methodology in [12].

The bridge has been divided into sectors: the central span has been decomposed into five sectors, while the two lateral ones into three sectors each; in addition, one sector has been assigned to each abutment and pier. The average value of the ascending and descending LOS measurements of the PSs falling within each sector has been assigned to its centroid (Figure 3) for all the acquisition dates in the time window common to the ascending and descending datasets. The time series thus obtained are temporally relative to the first common date to the two stacks of images.

The operations described, consisting of interpolations in space and time, make the ascending and descending datasets consistent, in order to allow the decomposition of the displacement components.

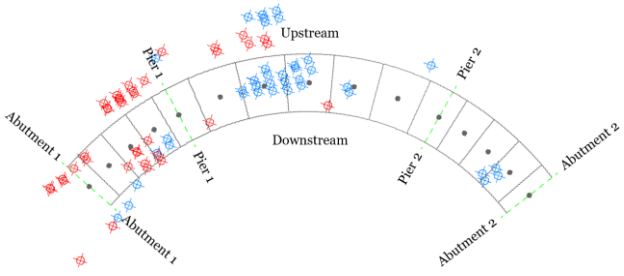

Figure 3 Subdivision of the bridge deck into sectors. The PSs detected in ascending geometry are red, while the ones identified in descending geometry are blue.

Since the trend of the LOS displacements of the PSs characterized by permanent deformations has opposite sign in ascending and descending geometries, it is reasonable to suppose that the real displacement vectors have a prevailing horizontal component with respect to the vertical one. Consequently, a horizontal deformation plane has been assumed for the calculation of the actual displacement components. Since the bridge is curved and therefore there are no longitudinal and transverse axes representative for its entire planimetric development, East and North have been chosen as the reference directions along which the displacement components are derived. Knowing the directions of the ascending and descending LOS, the real displacement component estimates $\hat{d}_E$ and $\hat{d}_N$, along the East and North direction respectively, have been calculated for each sector and for each date in the time window by solving the following linear system of two equations in two unknowns:

$$\mathbf{d}_{\mathrm{LOS}} = \mathbf{B}\,\hat{\mathbf{d}} \tag{1}$$

where

$$\mathbf{d}_{\mathrm{LOS}} = \begin{Bmatrix} d_A \\ d_D \end{Bmatrix},\ \mathbf{B} = \begin{bmatrix} \sin\theta_A \cos\alpha_A & -\sin\theta_A \sin\alpha_A \\ \sin\theta_D \cos\alpha_D & -\sin\theta_D \sin\alpha_D \end{bmatrix},\ \hat{\mathbf{d}} = \begin{Bmatrix} \hat{d}_E \\ \hat{d}_N \end{Bmatrix}$$

d_A and d_D are the measurements along the ascending and descending LOS, θ is the incidence angle of the LOS and α is the angle between the LOS horizontal projection and the East axis (Figure 4). Table 1 summarizes the values of the angles θ and α which define the direction of the ascending and descending LOS over the area where the bridge stands. The displacement estimates are affected by uncertainties that comprise a systematic and a random component.

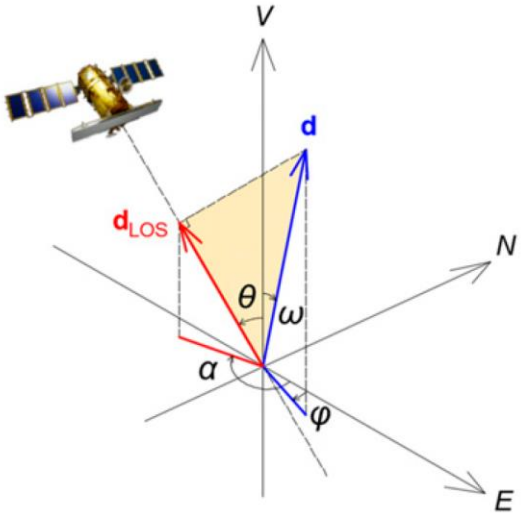

Figure 4 Scheme representing a hypothetical real displacement vector, **d**, and its component detected by the SAR sensor along the Line-Of-Sight, $\mathbf{d}_{\mathrm{LOS}}$.

Table 1 Characteristics of ascending and descending LOS of COSMO-SkyMed sensors in the area of interest.

Geometry	θ [degrees]	α [degrees]
Ascending	26.693	169.472
Descending	34.031	11.549

The systematic error depends on the three-dimensional nature of the real displacement vector versus the two-dimensional displacement estimate, therefore it appears if the actual neglected displacement component perpendicular to the assumed deformation plane is actually different from zero. The random error is instead always present and related to the accuracy of the starting LOS measurements. The difference between the estimated and real values of the displacement component along the *i*-th direction (East or North), i.e. the total error, has been calculated using the following equation (where the first term on the right-hand side is the systematic error and the second one represents the random error):

$$\hat{d}_i - d_i = c_i \cdot d_\perp \pm \varepsilon_i \cdot \delta \cdot \sigma \tag{2}$$

where $d_\perp$ is the actual neglected displacement component orthogonal to the horizontal deformation plane (vertical component), δ is a coefficient defining the level of confidence for $\hat{d}_i$, σ is the standard deviation of the LOS measurements, and c_i and ε_i are error coefficients depending on the direction of the LOS and of $\hat{d}_i$.

For the present case, to compute the total error it was assumed the existence of a real vertical displacement component $d_\perp = d_V = \pm 10$ mm, a confidence level of 90% was chosen (δ = 1.65), and σ has been set equal to 2 mm [20]. Furthermore, the error coefficients assume the following values: c_E = -0.34, c_N = -9.06, ε_E = 1.47, ε_N = 7.45. It is worth noting that the coefficients associated to the North component are higher than the other ones. This is because the satellites are on near-polar orbits and the LOS is orthogonal to the orbit, therefore the measurements are not very sensitive to deformations in North-South direction, thus increasing the degree of uncertainty along this direction.

The deformed configuration of the bridge deck related to the last acquisition date of the monitoring period is shown in Figure 5 and represents the movements of the deck occurred during the four years of InSAR monitoring. It has been reconstructed by combining the East and North displacement components for the sectors in which at least one PS for both acquisition geometries has been identified. The deformations obtained, even if not covering the entire deck and taking into account the uncertainties on the displacement estimates, are compatible with the effects on the bridge of the thrust exerted by the landslide slope. In particular, the permanent displacement of the sector corresponding to abutment 1, founded on the slope affected by the slow-moving landslide, is evident (the estimated horizontal displacement is about 175 mm in the four years of monitoring).

4 AEM modelling

The Applied Element Method (AEM) consists in modelling a structure as an assembly of small 3D rigid elements (with 6 degrees-of-freedom) connected along their surfaces through a set of normal and shear springs. The springs represent continuity between elements, reflect the properties of the various materials constituting the structure and allow to derive the stresses and strains fields. For

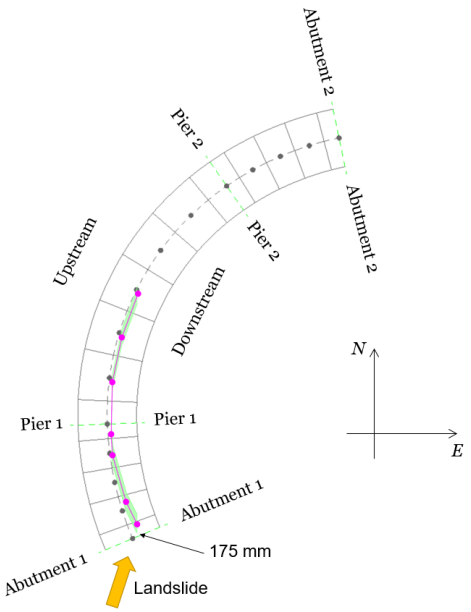

Figure 5 Reconstruction of the deformed configuration of the bridge deck in the horizontal plane on December 30th, 2021, taking into account the uncertainty bands for both East and North displacement components. The dots represent the centroids of the various sectors and displacements are plotted in 10:1 scale.

example, to model a reinforced concrete structure as the bridge under examination, two types of springs are employed: the matrix springs, which represent the concrete material, and the reinforcement springs, which reproduce the presence of the rebars, in terms of dimension, position and material properties. Non-linear and path-dependent constitutive models are in fact assigned to the springs in order to reproduce the behaviour of the various materials composing the structure. Furthermore, another type of normal and shear springs, called contact springs, are generated when elements come into contact with each other or with the ground, allowing modelling the occurring transfer of energy.

The AEM model of the curved roadway bridge (Figure 6), consisting of approximately 37,000 elements, has been built using the software Extreme Loading for Structures (ELS) [21]. Two types of concrete (one for the deck and one for piers and abutments) and two types of steel (one for the ordinary rebars and one for the post-tensioned cables) have been considered in the modelling. The deck and the upper part of the piers have been modelled in detail, reflecting the characteristics of the real bridge in terms of both geometry and arrangement of the rebars. Regarding the 27 post-tensioned cables (each consisting of 42Ø7), the springs that represent them follow the development known from the design tables and have been tensioned with a pre-stress equal to the design value of the final tension. The abutments and the foundations of the piers, which are fixed to the ground, have been instead built in a simplified way, choosing a less complex geometry than their physical counterpart and not including the reinforcements in the model. The asphalt layer and the concrete curbs have not been directly modelled, but their own weight has been taken into account assigning a corresponding increased equivalent density to the elements at the extrados of the deck.

As previously mentioned, the behaviour of the materials has been taken into account by assigning appropriate constitutive models to the springs. The Maekawa model [22] has been used to describe the concrete constituting the deck and the piers and the Menegotto-Pinto model [23] has been used instead to model the steel reinforcements. The simplified modelling of the abutments and the piers foundations involved using a linear model for the springs of the elements that compose them, while a bearing model has been assigned to the springs at the interface between abutment 1 and the deck, in order to reproduce the sliding in the horizontal plane allowed by the mobile constrain.

The adopted material models have been defined by assigning them a set of parameters, some of which have been subject to calibration in order to reproduce through

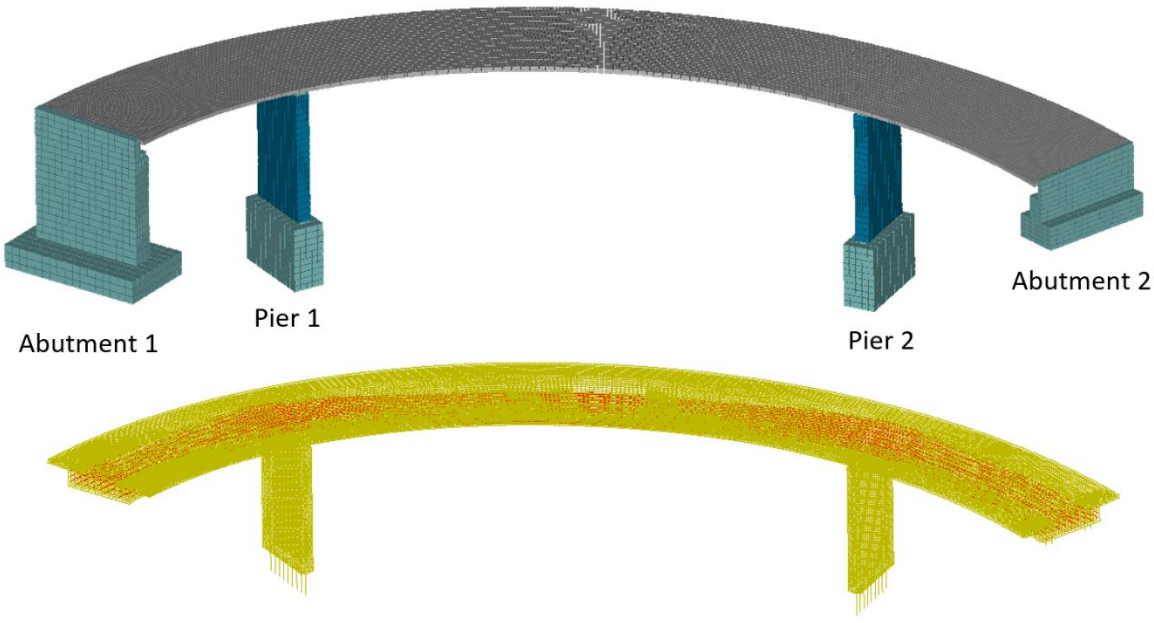

Figure 6 AEM model of the curved roadway bridge. Above, detail of the model mesh; below, reinforcement implemented in the model: the ordinary reinforced bars are in yellow, while the post-tensioned cables are represented in red.

Table 2 Material properties adopted for the calibrated model. E and G are the Young and shear modulus; f_c and f_t represent the compressive and tensile strength, while τ_0 is the shear strength; σ_y and σ_u are the yield and ultimate stress. All values are expressed in MPa.

Structural element type	E	G	f_c	f_t	τ_0	σ_y	σ_u
Deck	37500	14583	40	3	7.35	-	-
Piers	30000	12500	30	3	7.35	-	-
Reinforcing bars	200000	80000	-	-	-	431.5	561
Post-tensioned cables	200000	80000	-	-	-	1370	1570
Abutments and piers foundations	2600000	1000000	5000	5000	3000	-	-
Abutment 1-deck connection	200000	1716	40	-	-	-	-

the modelling the dynamic behaviour of the real bridge as faithfully as possible. The calibration has been performed referring to the results of Ambient Vibration Tests (AVTs) carried out during an in situ experimental campaign to assess the dynamic behaviour of the curved roadway bridge. Acceleration measurements have been processed using MOVA, a recently developed software for Operational Modal Analysis [24] that has allowed deriving the dynamic identification of the bridge in terms of modal parameters, i.e. natural frequencies, damping ratios and mode shapes.

The calibration of the model has been carried out by comparing natural frequencies and mode shapes of the first three modes experimentally identified with the numerical predictions obtained from the modal analysis of the AEM model of the bridge, varying the material stiffness of some structural parts in terms of Young and shear moduli of the constitutive models. In particular, the Young and shear moduli of the concrete of the deck and piers and the shear modulus of the bearing material at the interface between abutment 1 and the deck have been updated in the calibration. Starting from the values corresponding to the types of concrete prescribed in the original design (concrete C32/40 for the deck and C25/30 for the piers), the parameters have been varied in order to minimize the difference between the experimental and model-estimated frequencies of the three considered modes. A percentage relative error, expressed by the following formula, has been calculated for each mode:

$$\varepsilon = \frac{f_{exp} - f_{\mathrm{AEM}}}{f_{exp}} \cdot 100 \qquad (3)$$

Table 3 Experimental and AEM model-predicted modal frequencies of the first three mode, and corresponding percentage relative error.

Mode ID	f_{exp} [Hz]	f_{AEM} [Hz]	ε [%]
1	2.3737	2.3148	2.48
2	5.8600	5.6406	3.74
3	6.5049	6.4295	1.16

where f_{exp} is the experimental frequency, while f_{AEM} is the frequency predicted with the modal analysis of the AEM model of the bridge.

The final values of the parameters obtained at the end of the calibration process are summarized in Table 2. For the calibrated model, percentage relative errors lower than 4% have been achieved, as summarized in Table 3.

Comparing instead the mode shapes, represented in Figure 7, for the first mode a high consistency between experimental and numerical results has been obtained, while for the second and third modes the mode shapes predicted through the modal analysis do not completely match the ones derived from the AVTs, especially with regard to the horizontal movements. This partial disagreement can be explained by the complex geometry of the curved bridge, as well as by considering that the dynamic tests have been carried out on a structure already deformed and damaged due to the effects of the landslide, while the model reproduces the design configuration not affected by the landslide-induced movements.

In order to replicate the actual condition of the bridge in terms of deformation, damage and modifications of the bearing supports, a displacement input has been applied at the boundaries of the AEM model to simulate the progression of the landslide. In particular, a horizontal displacement of 200 mm has been applied in the direction of maximum slope towards abutment 1 and the foundation of pier 1. The computational deformed configuration thus obtained reproduces quite faithfully the current state of the bridge observed on site, as shown in Figure 8. Going more into detail, the numerical analysis has predicted the closure of the joints of both abutment 1 and abutment 2 consistently with the real situation, and the longitudinal and transverse rotations of pier 1 and pier 2 are also well simulated, in line with what found on site. In particular, the rotation around the transverse axis of the deck, activated due to the pendulum behaviour of the piers, is in opposite directions for pier 1 and pier 2, while, for both the piers, the longitudinal rotation has led to a partial loss of support due to the lifting of the downstream side of the piers.

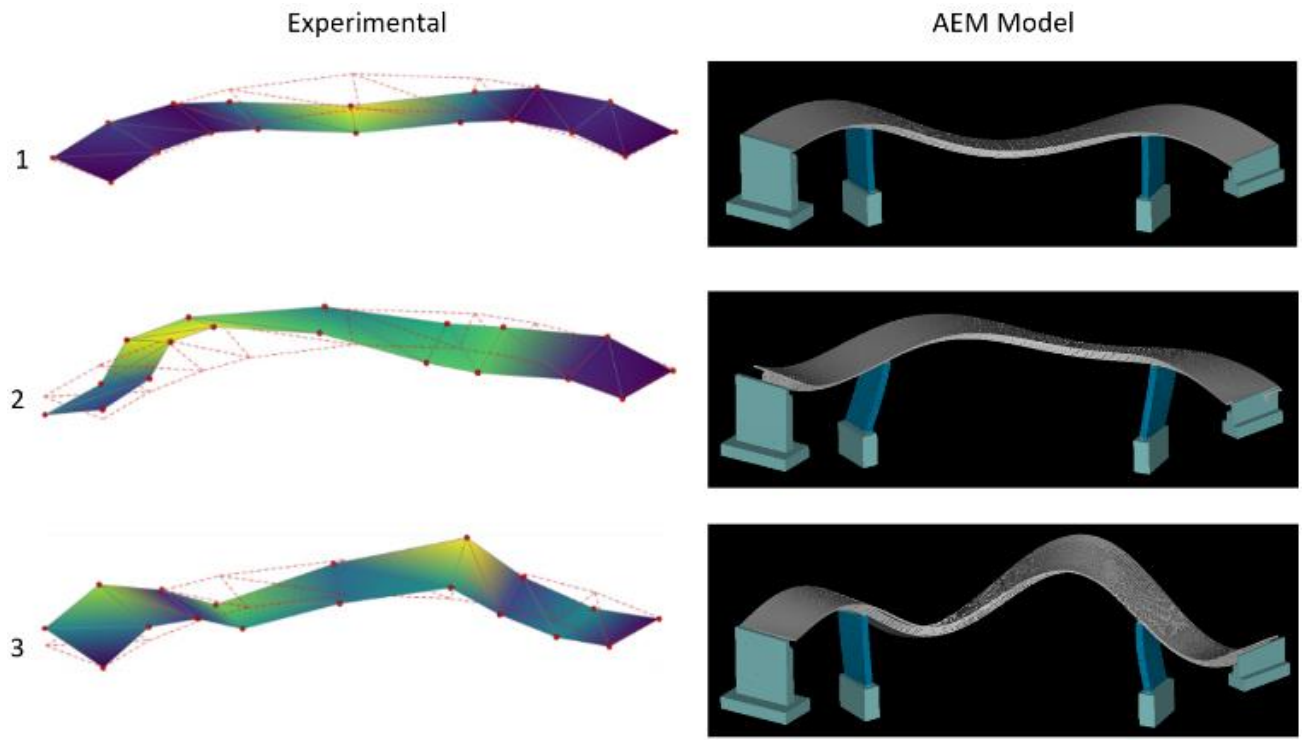

Figure 7 Comparison between experimental and numerical mode shapes for the first three modes.

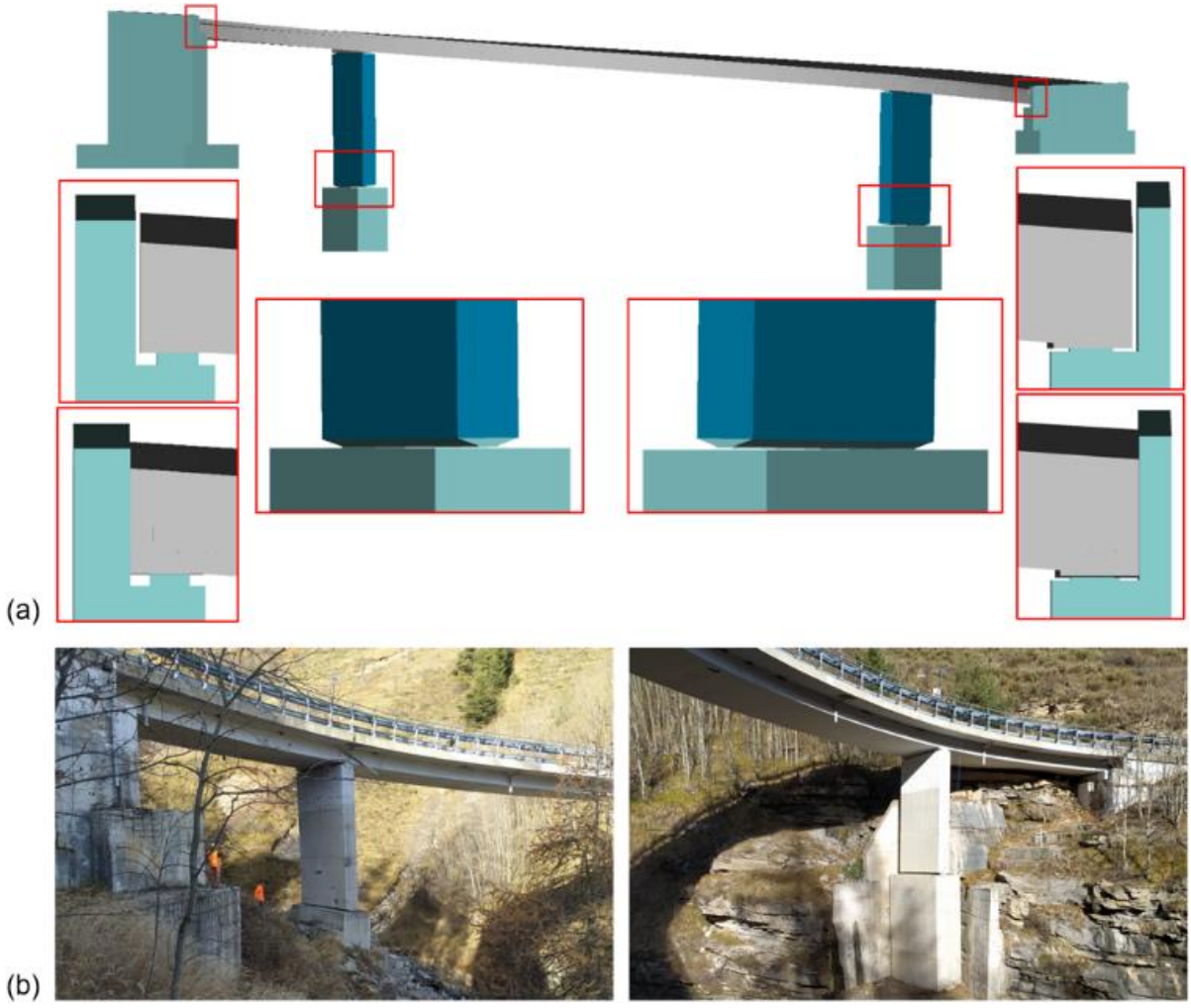

Figure 8 (a) Deformed configuration of the AEM model; the focus on the abutments show the situation before and after the application of the displacement input. (b) Current condition of the bridge observed on site, with details of pier 1 (on the left) and pier 2 (on the right).

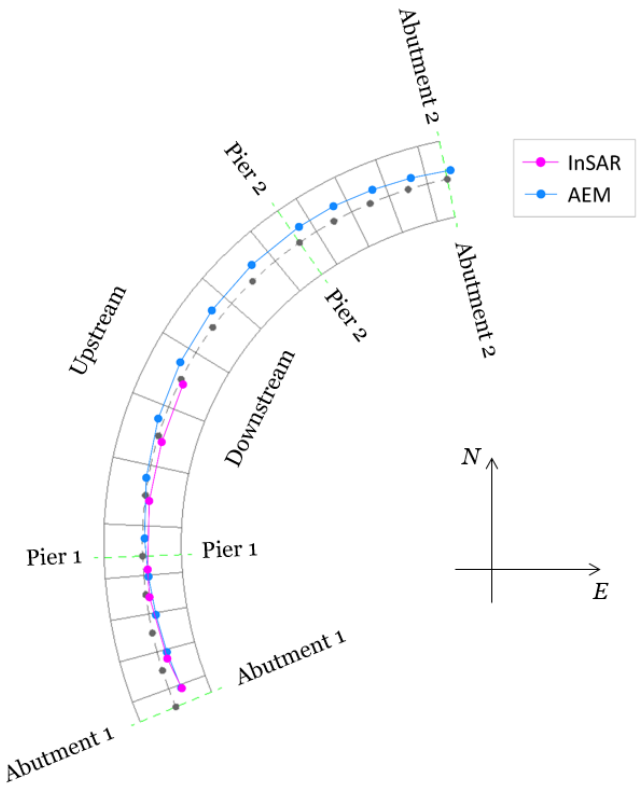

Figure 9 Comparison between the deformed configuration reconstructed from InSAR analysis on December 30th, 2021 and that derived from AEM numerical simulation. Displacements are plotted in 10:1 scale.

5 Combination of InSAR and AEM analyses

A quantitative comparison between the values of the deck displacements obtained through InSAR analysis and those derived from AEM numerical simulation has not currently been performed, given that the satellite monitoring time window covers four years (from 2018 to 2021), while numerically predicted deformations concern the time span from the construction of the bridge to the present day. It is also worth remembering that the extent of the total displacements of the landslide slope is not known, therefore the input given to the numerical model is only an approximate estimate. For this reason, it was possible to compare only qualitatively the results of the two analyses.

The numerically predicted East and North displacement components have been extrapolated for the elements corresponding to the position of the centroids of the various sectors, and their values have been scaled in order to match the North displacement of the centroid corresponding to abutment 1 with that reconstructed from InSAR processing for the last acquisition date. As shown in Figure 9, for the portion of the deck between abutment 1 and pier 1, the two deformed configurations almost coincide. The fact that, for abutment 1 centroid, not only the North component (imposed) but also the East one is the same for both reconstructions, suggests that the hypothesis on the direction of the displacement input applied to the model, i.e. the horizontal projection of the maximum slope of the versant, can be considered correct. For the deck part between pier 1 and pier 2 for which it was possible to carry out InSAR reconstruction, it can be noted that, while the East displacement components obtained with InSAR and AEM analyses are very similar for each centroid, the North components exhibit some differences. This result can be related to the higher uncertainty of the InSAR-deduced displacements along the North-South direction and could therefore fall within the error committed in their estimates.

The next step of this study will be to update the AEM model considering the modifications produced on the real bridge due to the interventions. Subsequently, a collapse simulation will be performed on the updated bridge, already deformed during the previous loading stage, by applying increasing horizontal displacements to abutment 1 and pier 1 foundation until reaching the failure. The collapse conditions obtained from the numerical analysis, in terms of displacements of a representative control node, will be used to setup alert thresholds for displacement measurements derived from InSAR monitoring, useful to help decision-makers take any measures in order to minimize risks.

6 Conclusions

This paper has presented an application of a multidisciplinary strategy for the structural assessment of bridges affected by slow deformation phenomena, based on the combination of InSAR-based Structural Health Monitoring and numerical simulations with the Applied Element Method.

The examined case study is a curved roadway bridge in Italy, undergoing slow movements induced by a landslide affecting the slope on which one of its abutments and one of its piers are founded. The area where the bridge is located is monitored by the satellite constellation COSMO-SkyMed. SAR images acquired from 2018 to 2021 have been processed through PSP technique and post-processed, in order to obtain the displacements of the bridge deck in the horizontal plane over time. The results have allowed to highlight a permanent deformation of the portion of the deck between the abutment and the pier directly affected by the landslide, probably related to its effect on the structure. An AEM numerical model of the bridge has been built referring to the original design documents and calibrated using the results of the dynamic identification with Ambient Vibration Tests. A numerical analysis has been performed applying to the model a displacement input representing the effects of the thrust exerted by the landslide slope on the structure. The simulation has reproduced a deformed configuration in good agreement with the actual deformed shape and damaged condition of the bridge. Moreover, the computationally predicted displacements of the deck are qualitatively consistent with InSAR measurements, allowing an interpretation of the latter from a structural engineering point of view. The collapse simulation and the definition of alert thresholds for InSAR measurements is left to the continuation of the research.

It is concluded that the integration of information derived from InSAR monitoring and AEM analysis contributes to the understanding of the effects that the progression of slowly-evolving deformation phenomena has on bridges, providing relevant elements for their structural assessment, and therefore for guiding preventive maintenance interventions and other actions aimed at mitigating risks.

Acknowledgement

The Authors would like to acknowledge the support of FABRE consortium (https://www.consorziofabre.it/en/homepage/), the Italian research consortium for the assessment and monitoring of bridges, viaducts and other structures. Authors from UNIPG also acknowledge funding by the European Union - NextGenerationEU under the Italian Ministry of University and Research (MUR) National Innovation Ecosystem grant ECS00000041 - VITALITY.

References

[1] Xu, C.; Ni, Y.Q.; Wang, Y.W. (2022) *A novel Bayesian blind source separation approach for extracting non-stationary and discontinuous components from structural health monitoring data*. Eng Struct 269, 114837

[2] Anastasopoulos, D.; De Roeck, G.; Reynders, E.P.B. (2021) *One-year operational modal analysis of a steel bridge from high-resolution macrostrain monitoring: Influence of temperature vs. retrofitting*. Mech Syst Signal Process 161, 107951

[3] Pallarés, F.J.; Betti, M.; Bartoli, G.; Pallarés, L. (2021) *Structural health monitoring (SHM) and Nondestructive testing (NDT) of slender masonry structures: A practical review*. Constr Build Mater 297, 123768

[4] Meixedo, A.; Ribeiro, D.; Santos, J.; Calçada, R.; Todd, M. (2021) *Progressive numerical model validation of a bowstring-arch railway bridge based on a structural health monitoring system*. J Civ Struct Heal Monit 112, 11, pp. 421–449.

[5] Sharma, S.; Sen S. (2021) *Bridge Damage Detection in Presence of Varying Temperature Using Two-Step Neural Network Approach*. J Bridg Eng 26, 6, 04021027.

[6] Zhu, M.; Wan, X.; Fei, B.; Qiao, Z.; Ge, C.; Minati, F.; et al. (2018*) Detection of building and infrastructure instabilities by automatic spatiotemporal analysis of satellite SAR interferometry measurements*. Remote Sens 10, 11.

[7] Cavalagli, N.; Kita, A.; Falco, S.; Trillo, F.; Costantini, M.; Ubertini, F. (2019) *Satellite radar interferometry and in-situ measurements for static monitoring of historical monuments: The case of Gubbio, Italy*. Remote Sens Environ 235, 111453.

[8] Mele, A.; Miano, A.; Di Martire, D.; Infante, D.; Ramondini, M.; Prota, A. (2022) *Potential of remote sensing data to support the seismic safety assessment of reinforced concrete buildings affected by slow-moving landslides*. Arch Civ Mech Eng 22.

[9] Giordano, P.F.; Turksezer, Z.I.; Previtali, M.; Limongelli, M.P. (2022) *Damage detection on a historic iron bridge using satellite DInSAR data*. Struct Heal Monit 21, pp. 2291–2311.

[10] Qin, X.; Ding, X.; Liao, M.; Zhang, L.; Wang, C. (2019) *A bridge-tailored multi-temporal DInSAR approach for remote exploration of deformation characteristics and mechanisms of complexly structured bridges*. ISPRS J Photogramm Remote Sens 156, pp. 27–50.

[11] Schlögl, M.; Widhalm, B.; Avian, M. (2021) *Comprehensive time-series analysis of bridge deformation using differential satellite radar interferometry based on Sentinel-1*. ISPRS J Photogramm Remote Sens 172, pp. 132–146.

[12] Farneti, E.; Cavalagli, N.; Costantini, M.; Trillo, F.; Minati, F.; Venanzi, I.; Ubertini, F. (2022) *A method for structural monitoring of multispan bridges using satellite InSAR data with uncertainty quantification and its pre-collapse application to the Albiano-Magra Bridge in Italy*. Struct Heal Monit 22, 1.

[13] Meguro, K.; Tagel-Din, H. (1997) *A new efficient technique for fracture analysis of structures*. Bull Earthq Resist Struct Res Center, IIS, Univ Tokyo, pp. 103–116.

[14] Tagel-din, H.; Meguro, K. (1999) *Applied element simulation for collapse analysis of structures*. Bull Earthq Resist Struct Res Ctr, pp. 113–123.

[15] Meguro, K.; Tagel-Din, H. (2002) *Applied Element Method Used for Large Displacement Structural Analysis*. J Nat Disaster Sci 24, pp. 25–34.

[16] Mahrous, A.; Ehab, M.; Salem, H. (2020) *Progressive collapse assessment of post-tensioned reinforced concrete flat slab structures using AEM*. Eng Fail Anal 109, 104278.

[17] Garofano, A.; Lestuzzi, P. (2016) *Seismic Assessment of a Historical Masonry Building in Switzerland: The "Ancien Hôpital De Sion."* Int J Archit Herit 10, pp. 975–992

[18] Scattarreggia, N.; Salomone, R.; Moratti, M.; Malomo, D.; Pinho, R.; Calvi, G.M. (2022) *Collapse analysis of the multi-span reinforced concrete arch bridge of Caprigliola, Italy*. Eng Struct 251, 113375.

[19] Salem, H.M.; Helmy, H.M. (2014) *Numerical investigation of collapse of the Minnesota I-35W bridge*. Eng Struct 59, pp. 635–645.

[20] Costantini, M.; Falco, S.; Malvarosa, F.; Minati, F.; Trillo, F.; Vecchioli, F. (2014) *Persistent scatterer pair interferometry: Approach and application to COSMO-skymed SAR data*. IEEE J Sel Top Appl Earth Obs Remote Sens 7, pp. 2869–2879.

[21] Applied Science International LLC. Extreme Loading for Structures (2020).

[22] Maekawa, K.; Okamura, H. (1983) *Deformational Behavior and Constitutive Equation of Concrete Using the Elasto-Plastic and Fracture Model*. J Fac Eng Univ Tokyo, Ser B, 37, pp. 253–328.

[23] Menegotto, M.; Pinto, P.E. (1973) *Method of Analysis for Cyclically Loaded R. C. Plane Frames Including Changes in Geometry and Non-Elastic Behavior of Elements under Combined Normal Force and Bending*. Proc IABSE Symp Resist Ultim Deform Struct Acted by Well Defin Loads, pp. 15–22.

[24] García-Macías, E.; Ubertini, F. (2020) *MOVA/MOSS: two integrated software solutions for comprehensive structural health monitoring of structures*. Mech Syst Signal Process, 143, 106830.